Appl. Phys. A 75, 229–235 (2002)
DOI: 10.1007/s003390201334

Applied Physics A
Materials Science & Processing

A.M. SONG[1,2,3,✉]

Electron ratchet effect in semiconductor devices and artificial materials with broken centrosymmetry

[1] Sektion Physik der Ludwig-Maximilians-Universität, Geschwister-Scholl Platz 1, 80539 München, Germany
[2] Division of Solid State Physics and Nanometer Structure Consortium, Lund University, 221-00 Lund, Sweden
[3] Department of Electrical Engineering and Electronics, UMIST, Manchester M60 1QD, UK

Received: 16 January 2002/Accepted: 11 February 2002
Published online: 22 April 2002 • **© Springer-Verlag 2002**

ABSTRACT Studies on nonlinear electron transport in nanometer-sized semiconductor devices with broken centrosymmetry are reviewed. In these devices, an applied alternating (rocking) electric field induces a net flow of electrons in the direction perpendicular to that of the applied field. Such an electron ratchet effect has been observed in a number of differently designed devices, fabricated from two types of semiconductor material systems. The functionality is interpreted with an extended Büttiker–Landauer formula. We show that the devices operate at both cryogenic and room temperatures and at frequencies up to at least 50 GHz. Based on a similar microscopic mechanism, we have also constructed, to the best of our knowledge, the first artificial electronic nanomaterial that operates at room temperature. The promising possibilities for practical applications, such as rectification, microwave detection, second-harmonic generation, etc., are also discussed.

PACS 73.23.Ad; 73.40.Ei; 73.50.Fq; 81.05.Zx; 07.57.Kp

1 Introduction

When a system with a broken spatial symmetry is taken out of equilibrium by, for example, introducing an external fluctuation (i.e. the time average is zero), a net flow of particles along a certain direction may occur [1–9]. A simple way to observe this ratchet effect is to construct a one-dimensional, periodic, asymmetric (typically sawtooth-like) potential. In operation, both the external fluctuation force and the generated net flow of particles are along the potential-modulation direction. The ratchet effect has been suggested to be an underlying mechanism of some biological phenomena, such as molecular motors [1, 2, 7, 10]. Recently, several groups have invented devices consisting of arrays of symmetry-breaking microscopic obstacles and used them to sort biomolecules [11–14]. This shows that asymmetric geometries may provide the same functionality as asymmetric potentials in creating a guided flow of particles.

There are also ratchets in which the mobile particles are electrons. Electron ratchets may exist naturally or can be constructed artificially. It was discovered more than 30 years ago that some natural crystals can generate direct electron currents under uniform illumination [15–17]. Referred to as the photovoltaic effect, the phenomenon has been identified as being a macroscopic manifestation of the lack of centrosymmetry in the microscopic elemental structure, despite the macroscopic homogeneity of these crystals. In this case, light serves as a source of external fluctuation by imposing an unbiased, time-periodic electric field on the crystals, and the generation of direct electron current can be viewed as extremely fast rectification, or a ratchet effect, at the light frequency. One difference compared with a one-dimensional ratchet is that the generated electron current may flow in a direction different from, or even perpendicular to, that of the driving electric field of the light. This is due to the broken symmetry of the microscopic potential in two or three dimensions. With the high spatial resolution of modern semiconductor fabrication technologies, it is possible to make different types of artificial electron ratchets in well-controlled ways. Direct voltages or currents induced by rocking electric fields have been observed at THz frequencies [18], in electron billiard structures [19], and in the quantum transport regime [20, 21].

Here, our recent work on the ratchet effect, realized in nanometer-sized electron billiard structures, is reviewed. In our devices, instead of introducing asymmetric, sawtooth-like ratchet potentials, only the device geometries (or shapes) are tailored to break the spatial reversion symmetry. The electron transport is ballistic, i.e. the sizes of the devices are smaller than the electron scattering length, l_e, and the electrons in the devices are mainly scattered from the designed device boundary rather than by randomly distributed impurities [22]. The observed nonlinear effect is so strong that the devices are capable of rectification applications and are hence called ballistic rectifiers. The devices generally have four terminals or electric contact leads. When a regular ac voltage or a random signal is applied via two of the electrical contact leads, a direct voltage or current is generated and can be measured through the other two terminals. This is similar to the operation of a bridge rectifier, but our devices have a completely different working principle. Not only do they operate at cryogenic temperatures, our smallest devices have also been shown to work at room temperature, with a rectification efficiency reaching 14%. Our recent experiments have also demonstrated that the ballistic rec-

✉ *Current and permanent address*: Department of Electronical Engineering and Electronics, UMIST, PO Box 88, Manchester M60 1QD, UK. Fax: +44-161/2004770, E-mail: aimin.song@ftf.lth.se

tifiers function at frequencies up to at least 50 GHz and have a sensitivity to microwaves roughly as high as that of a commercial microwave-detection diode. Based on a similar microscopic mechanism, we have also constructed, to the best of our knowledge, the first artificial electronic nanomaterial that operates at room temperature. Some promising possibilities for practical applications, such as rectification, microwave detection, higher harmonic generation, etc., will be discussed.

2 Experiments on GaAs–AlGaAs-based ballistic rectifiers

Figure 1a shows an atomic force microscope image of the central part of one of the first ballistic rectifiers. Device fabrication starts with a modulation-doped GaAs–AlGaAs heterostructure with a two-dimensional electron gas located 37 nm below the wafer surface. The electron density is about $5\times10^{11}\ \mathrm{cm}^{-2}$ and the mobility about $5\times10^{5}\ \mathrm{cm}^2\,\mathrm{V}^{-1}\,\mathrm{s}^{-1}$ at a temperature of $T = 4.2$ K, giving $l_e = 5.8\ \mu$m. Following the pattern definition by electron-beam lithography, the dark areas in Fig. 1a are etched and become nonconductive for electrons. As a result, the triangular antidot is defined in the cross-junction formed by the two narrow channels (labeled "source" S and "drain" D) and the two wide channels (labeled "upper" U and "lower" L).

Since l_e is larger than the central part of the device, specular electron scattering from the etched boundaries dominates the transport properties. It is therefore possible to alter the device properties in the ballistic electron transport regime by simply changing the shape of the device (as will be shown below). This is in contrast to the case of the diffusive electron transport in devices much larger than l_e, where an electron current consists of electrons undergoing a large number of scattering events with, for example, randomly distributed impurities, and the electron transport is not sensitive to a change in device shape.

In our experiments, we apply current to leads S and D, and we detect the output voltage via L and U. The typical electron trajectories, illustrated by the arrows in Fig. 1a, suggest an accumulation of electrons in the lower lead and hence a negative voltage between L and U. Obviously, this cannot happen when the applied voltage or current is zero, since the same number of electrons travel along the opposite directions of the arrows. For a nonzero applied current, $I_{SD} \neq 0$, however, as shown by a detailed model [23, 24], the electron transmission along the arrows in Fig. 1a is changed by the applied electric field, while the transmission in the reversed direction is virtually unaffected. This gives rise to a finite negative voltage between L and U, V_{LU}.

The mirror symmetry along the central L–U axis results in

$$V_{LU}(I_{SD}) = +V_{LU}(-I_{SD})\ . \tag{1}$$

Correspondingly, $R_{SD,LU}(I_{SD}) = -R_{SD,LU}(-I_{SD})$, where the four-terminal resistance $R_{SD,LU} = V_{LU}/I_{SD}$. Such a picture is almost perfectly supported by the experimental V_{LU} vs. I_{SD} curve at $T = 4.2$ K, shown in Fig. 2. The slight deviations from (1) are attributed to unintentional breaking of the desired symmetry along the L–U axis by the imperfection of the fabrication. Any imperfection is expected to contribute a linear term to the V_{LU} vs. I_{SD} curve. This is similar to a change of the value of one of the four resistors in an otherwise balanced resistor bridge.

In the I–V characteristic of a two-terminal nonlinear device, such as a diode, the nonlinearity always comes on top of a (often very large) linear term. For the ballistic rectifier with the four-terminal geometry, there can, however, be no linear term present in the relation between output voltage and applied current, as shown by (1). The striking nonlinearity is a result of the mirror symmetry along the U–L axis and the broken symmetry along the S–D axis. As will be shown in Sects. 4 and 5, this has quite a few advantages in practical applications.

Based on a similar working principle, other types of ballistic rectifiers can be designed. The inset in Fig. 3 shows schematically a device containing channels defined by gates rather than by chemical etching. Instead of introducing a symmetry-breaking triangular scatterer as in Fig. 1a, the mirror symmetry along the S–D axis is broken by the horn-shaped U and L channels. The measured V_{LU} vs. I_{SD} curves at different gate voltages. V_{GU}, applied between the gates and the upper lead, are plotted in Fig. 3. As expected, the same result is obtained when the gate voltages are applied using the lower lead as the ground. Because of the imperfection of the fabrication, the curves are not perfectly symmetric along the $I_{SD} = 0$ axis. Nevertheless, it is obvious that by increasing the negative gate voltage from -1.2 to -1.5 V, the nonlinear component of I–V curves increases, which can be explained by the model (6) in Sect. 3.

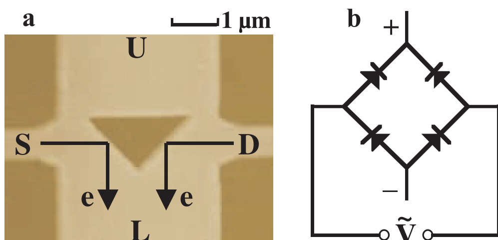

FIGURE 1 Atomic force microscope image of the central part of the device (**a**), which has a similar functionality to a bridge rectifier (**b**)

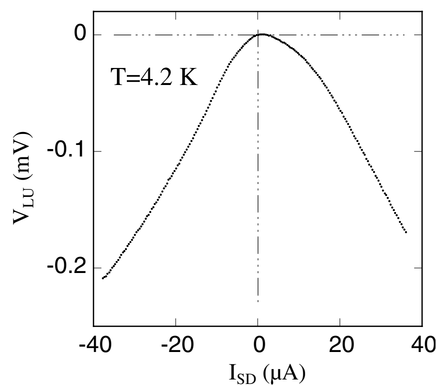

FIGURE 2 The output voltage between the lower and upper leads, V_{LU}, as a function of the input current through the source and drain leads, I_{SD}, measured at 4.2 K

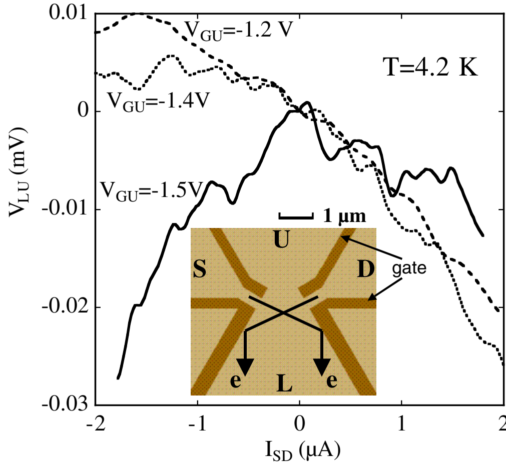

FIGURE 3 V_{LU} vs. I_{SD} curves at different gate voltages, V_{GU}, measured in a ballistic rectifier fabricated with gates rather than chemical etching, as schematically shown in the *inset*. The *dark areas* in the *inset* are gates, to which the same gate voltage is applied. The *arrows* in the *inset* illustrate typical electron trajectories

If an ac voltage is applied to leads S and D, as expected from the characteristics shown in Figs. 2 and 3, a negative average (dc) voltage can be observed between L and U. This will be demonstrated below using InP–InGaAs-based devices. Actually, a direct voltage output has been observed, even when an external noise signal is applied [25], showing a ratchet effect induced by the broken geometric symmetry and the guidance of ballistic electrons by the triangular antidot.

Because the device works similarly to a bridge rectifier (see Fig. 1b), it is called a ballistic rectifier. However, only a single device is used here, rather than four diodes as in the bridge rectifier. The mechanism is also entirely different, since no doping junction or barrier structure along the current direction is used in our devices. The pronounced nonlinear effect comes from the broken symmetry and the ballistic electron transport nature. As a result, as will be shown in Sect. 3, the ballistic rectifier has no intrinsic voltage or current threshold, and it can be used for the detection of very weak signals without the need of an external bias.

3 Model based on classical ballistic electron scattering

The Büttiker–Landauer formalism [26, 27], which treats transport in mesoscopic conductors as a transmission problem for carriers at the Fermi level, is widely used to describe the linear transport behavior of these conductors [28–34]. Recently, a rapidly increasing number of experimental [18, 20, 35–40] and theoretical [41–47] studies on nonlinear ballistic transport have been published. Nonlinearity is particularly important in mesoscopic conductors, because of the small device sizes and the fact that, in principle, nonlinearity can be induced by any non-zero applied current or voltage. By extending the Büttiker–Landauer formula to the nonlinear regime and the framework of classical ballistic electron scattering, we have obtained a model which provides analytical descriptions of the ballistic rectification effect [23].

For a mesoscopic conductor that is connected via perfect leads to a number of carrier reservoirs, the scattering approach yields the current through lead α:

$$I_\alpha = \frac{2e}{h}\sum_{\beta\neq\alpha}\int\left[f(E-\mu_\alpha)-f(E-\mu_\beta)\right] \times T_{\beta\leftarrow\alpha}(E,B)\mathrm{d}E\,. \tag{2}$$

Here, μ_α is the chemical potential of reservoir α and $f(E-\mu_\alpha)=\left[\exp\left(\frac{E-\mu_\alpha}{k_\mathrm{B}T}\right)+1\right]^{-1}$ is the Fermi–Dirac distribution function. $T_{\beta\leftarrow\alpha}(E,B)$ is the transmission coefficient for carriers from lead α to lead β at energy E and magnetic field B.

At $k_\mathrm{B}T=0$ and $B=0$, (2) becomes

$$I_\alpha = \frac{2e}{h}\sum_{\beta\neq\alpha}\overline{T}_{[\beta,\alpha]}(\mu_\alpha-\mu_\beta)\,. \tag{3}$$

Here, $\overline{T}_{[\beta,\alpha]}$ equals $\int_{\mu_\beta}^{\mu_\alpha} T_{\beta\leftarrow\alpha}(E,B)\mathrm{d}E/(\mu_\alpha-\mu_\beta)$ if $\mu_\alpha>\mu_\beta$, and $\int_{\mu_\alpha}^{\mu_\beta} T_{\alpha\leftarrow\beta}(E,B)\mathrm{d}E/(\mu_\beta-\mu_\alpha)$ otherwise. This shows that only the transmissions from reservoirs with higher chemical potentials to reservoirs with lower chemical potentials need to be considered.

As in the model for ballistic electron transport in a cross-junction by Beenakker and van Houten [48], the angular distribution of the ballistic electrons ejected from S and D, $P(\theta)$, largely determines the electron transmission probabilities into the L or U lead. In principle, the transmission coefficients at a finite value of I_{SD} should be obtained by first calculating the self-consistent potential in the device. Such a calculation is very complex. Instead, we consider there to be voltage drops at the entrances and exits of the S and D channels [46]. This only results in a change in the velocity component of an electron along the channel direction, v_x, by an amount of the mean velocity or drift velocity, Δv, while the velocity component in the perpendicular direction, v_y, is essentially not affected. The ejection angle of the electron changes from $\arctan(v_y/v_x)$ to $\arctan[v_y/(v_x\pm\Delta v)]$ at $I_{SD}=0$, meaning that the transmission probabilities of electrons into the L or U leads are directly related to the electron drift velocity, and hence I_{SD}, as is calculated and shown in Fig. 4. This is a particularly good approximation for this specific device geometry because the electron transmission probabilities are very sensitive to the ejection angles of the electrons. This allows (3) to be written as

$$I_\alpha \approx \frac{2e}{h}\sum_{\beta\neq\alpha}\overline{T}_{[\beta,\alpha]}(I_{[\beta,\alpha]})(\mu_\alpha-\mu_\beta)\,, \tag{4}$$

where $\overline{T}_{[\beta,\alpha]}(I_{\{\beta,\alpha\}})$ is equal to $\overline{T}_{\beta\leftarrow\alpha}(I_\alpha)$ if $\mu_\alpha>\mu_\beta$ and $\overline{T}_{\alpha\leftarrow\beta}(I_\beta)$ otherwise.

The relation between V_{LU} and I_{SD} is obtained via the four-terminal resistance

$$R_{SD,LU}\equiv\frac{V_{LU}}{I_{SD}}=\frac{3}{2}\frac{h}{e^2}\frac{\sin\theta_\mathrm{e}-\sin\theta_0}{2N_{LU}-3N_{SD}(1-\sin\theta_0)^2}\,, \tag{5}$$

where $\theta_\mathrm{e}=\theta_0+\arcsin[(\Delta v/v_\mathrm{F})\sin\theta_0]$, $\theta_0\approx\pi/4$ is the minimum ejection angle for an ejected electron to be scattered by the triangular antidot to the lower lead, v_F is the Fermi velocity, and N_{SD} and N_{LU} are the numbers of propagating modes

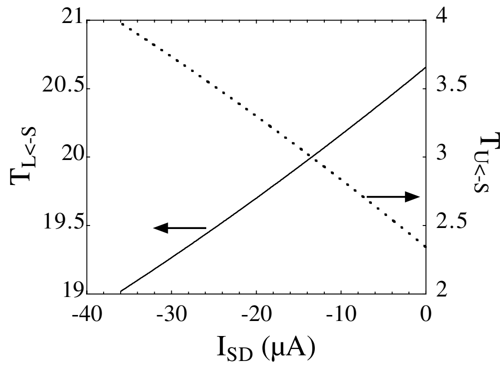

FIGURE 4 The calculated $T_{L\leftarrow S}$ and $T_{U\leftarrow S}$ as functions of the *negative* source–drain current

in channels S and D and channels L and U, respectively. The V_{LU} vs. I_{SD} curve, calculated analytically, is shown by the solid line in Fig. 5. It is in very good agreement with the experimental result (dashed line) especially in the low current regime, although there are no adjustable parameters at all in (5). At high currents, electron heating might take place and reduce the rectification effect, which is not included in the above model. Moreover, the length of the L and U channels (5 µm) is comparable to the electron mean free path, which results in some electrons changing direction before they pass through the channels and enter the electrical contact regions (carrier reservoirs). This certainly causes a reduced output.

It is interesting to note that in the limit of $I_{\mathrm{SD}}| \to 0$, V_{LU} is shown to have a quadratic response to I_{SD}:

$$V_{\mathrm{LU}} = -\frac{3\pi\hbar^2}{2e^3 E_{\mathrm{F}} N_{\mathrm{SD}}} \frac{(\sin 2\theta_0) I_{\mathrm{SD}}{}^2}{2N_{\mathrm{LU}} - 3N_{\mathrm{SD}}(1-\sin\theta_0)^2} . \quad (6)$$

Although the calculation is performed for the condition of $T = 0$, we can show that (6) is also valid for sufficiently small currents at finite temperature [49], meaning that there is no threshold voltage for the ballistic rectifier. There are a few advantages associated with the quadratic response, as will be discussed in Sect. 4. Equation (6) indicates that $|V_{\mathrm{LU}}|$ increases with decreasing E_{F}, N_{SD}, and N_{LU}, and this explains the enhancement of the nonlinearity with increasing negative gate voltage, as shown in Fig. 3. Based on the above picture, the nonlinear ballistic electron transport at finite magnetic fields can also be well described [50].

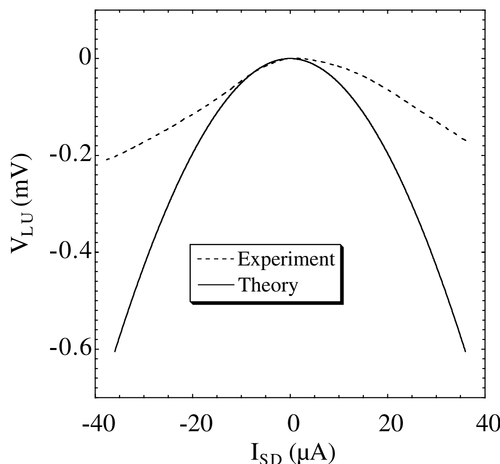

FIGURE 5 Theoretical (*solid line*) and experimental (*dashed line*, the same as that in Fig. 2) V_{LU} vs. I_{SD} curves for the device shown in Fig. 1a

4 InGaAs–InP-based room-temperature ballistic rectifiers

As the miniaturization of conventional semiconductor devices is approaching physical limits, great effort has been made to develop new types of nanodevices, which, from the application point of view, should operate at room temperature and GHz frequencies. The ballistic rectifier in Fig. 1a has already been demonstrated to work up to $T = 77$ K. To function at room temperature, a device size smaller than l_{e} (about 100 nm) at $T = 300$ K is required. This is, however, very difficult using a GaAs/AlGaAs heterostructure, due to the large depletion length (up to hundreds nm) close to etched device boundaries. The much shorter depletion length (below 30 nm) of the InGaAs–InP material system makes it possible to fabricate much smaller devices [51].

The inset of Fig. 6 shows an atomic force microscope image of one of the smallest devices that we have fabricated from a modulation-doped $\mathrm{In_{0.75}Ga_{0.25}As}$–InP quantum-well structure [52]. At room temperature, the density of the two-dimensional electron gas is $4.7 \times 10^{15}\,\mathrm{m^{-2}}$ and the mobility $1.2\,\mathrm{m^2\,V^{-1}\,s^{-1}}$, corresponding to $l_{\mathrm{e}} = 140$ nm. Since l_{e} is only slightly shorter than the distance from the left or right channel to the triangular antidot, most electrons can still travel this distance without being scattered. As shown by Hirayama et al. [53], if the electron transport is partially ballistic, the ballistic effect may still be observed, although it will be weaker than at low temperatures. In our experiment, instead of a dc current, we apply an ac voltage (1 kHz) to the device and measure the dc (or average) voltage between the lower and upper terminals. Indeed, a rectification efficiency of about 14%, roughly half of that at 100 K, is observed, as shown in Fig. 6. This is actually one of the very few types of novel nanodevices shown to work at room temperature so far.

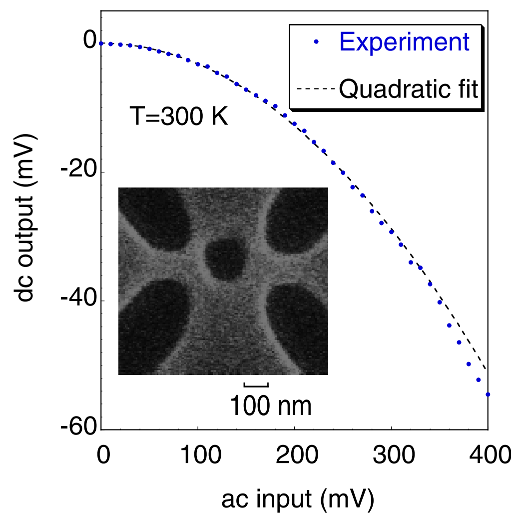

FIGURE 6 Room-temperature operation of one of the smallest ballistic rectifiers. The *inset* shows a scanning electron microscope image of the device. The frequency of the input ac signal is 1 kHz

Interestingly, at sufficiently low temperatures (not shown here), we have also observed that the output of smaller devices, such as the one in Fig. 6, changes sign, while the output of larger devices does not [54]. If a top gate is fabricated, one can actually switch the sign of the output by tuning the gate voltage.

We also perform high-frequency experiments up to 50 GHz. Because of the in-plane nature of the ballistic rectifier, i.e. the electrical contacts are laterally separated rather than placed on the front surface and the back (substrate), the parasitic capacitance between contacts is substantially lower than in a conventional vertical device of the same size. Furthermore, the new working mechanism does not rely on any minority carrier diffusion or barrier structure, two factors that also often limit the speed of conventional semiconductor diodes. The ballistic rectifier is therefore expected to function at very high frequencies. Figure 7 shows the dc output of the device versus the power of a 50-GHz signal at room temperature. Although we have not been able to test the devices at frequencies higher than 50 GHz so far, we expect, from the working principle, the cut-off frequency to be much higher, possibly up to hundreds of GHz or even in the THz regime.

It should be noted that the power (horizontal axis) in Fig. 7 is the output power from the signal source. Due to the impedance mismatch between the signal source (50 Ω) and the device (a few kΩ), as well as some power loss due to the cables at 50 GHz, effectively only a small fraction of the power from the signal source is actually applied to the device. It is estimated that the real sensitivity of the device is a few hundred mV output per mW input, which is virtually as high as that of a commercial microwave detection diode. We should point out that our devices have, however, not yet been specifically optimized. Much improvement can be expected in the future, by, for example, further reducing the device size. For a device about half the size of the one shown in Fig. 6, one can expect not only a much higher efficiency, but also stable performance that is insensitive to temperature changes up to room temperature.

The fit $y = ax^2$ (where y represents the dc output voltage, x the ac input voltage and a a constant) in Fig. 6 also supports the theoretical prediction of the quadratic response to input voltage (6). This allows second-harmonic signals to be generated without producing third or higher harmonics. The polarization of the generated second-harmonic signal (along the vertical direction) is perpendicular to that of the input signal (horizontal direction), which makes separation from the input signal much easier. Because of the quadratic nature, one would also expect the dc output to be a linear function of the applied microwave power, as is in fact demonstrated in Fig. 7.

5 Artificial nonlinear nanomaterials

Based on a working principle similar to that of the ballistic rectifier, we have designed a nanostructured material, constructed by the arrangement of nanometer-sized, symmetry-breaking elements into a two-dimensional lattice. Figure 8 shows an atomic force microscope image of the nanomaterial, fabricated from the same modulation-doped $In_{0.75}Ga_{0.25}As$–InP quantum-well structure, using electron-beam lithograph and chemical wet etching. Noticeably, the material is not a simple assembly of individual ballistic rectifiers. The offset introduced in neighboring columns of triangular antidots is crucial. The triangular antidots are placed in such a coherent way that neighboring antidots support each other by simultaneously scattering electrons and forming channels through which electrons are ejected. The typical electron trajectories, indicated by the arrows, suggest the accumulation of electrons in the upward direction. Indeed, the material generates a dc voltage between the lower and upper contacts when an ac voltage or electric field is applied to the left and right sides of the material, demonstrating an intrinsic nonlinear functionality [55].

As the nanomaterial is intrinsically nonlinear, individual devices can be made by simply cutting pieces from the material according to the requirements for different applications. Moreover, it is also possible to achieve room-temperature op-

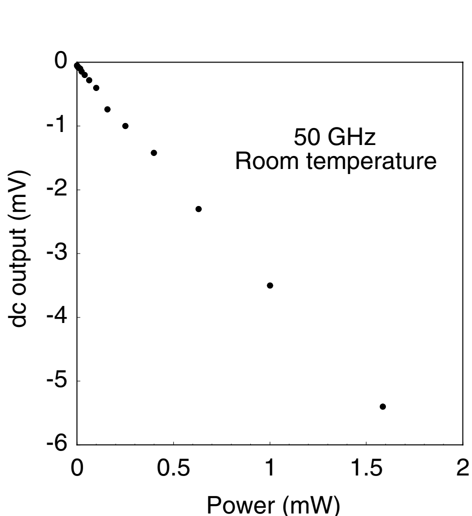

FIGURE 7 The output dc voltage of the device versus the power of the applied 50-GHz signal at room temperature

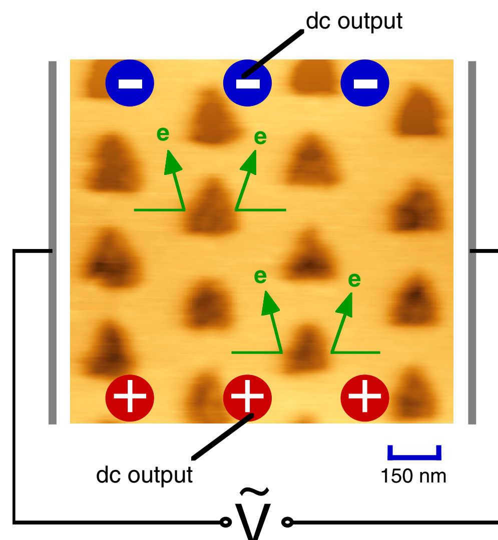

FIGURE 8 An atomic force microscope image of the nanomaterial. The *arrows* represent typical electron trajectories

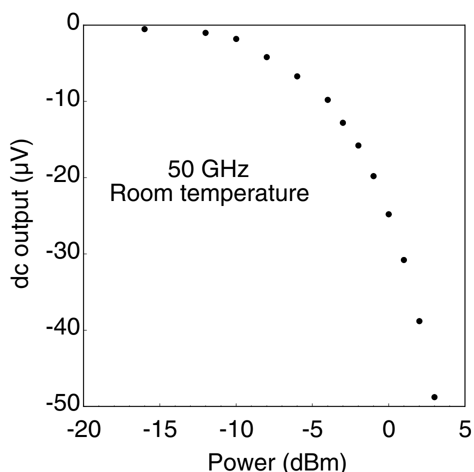

FIGURE 9 The output dc voltage of the nanomaterial versus the power of the applied 50-GHz signal at room temperature. The rf signal is applied to the material via coplanar probes

eration by fabricating nanomaterials with "lattice constants" comparable to, or shorter than, the electron mean free path. Similar to a ballistic rectifier, the in-plane nature of the nanomaterial ensures that the parasitic capacitance between contacts is much lower than in a conventional vertical device of the same size. The nanomaterial thus has an extremely high working speed, as is evident in high-frequency experiments. The curve in Fig. 9 shows the output dc voltage between the upper and lower contacts as a function of the rf power of a 50-GHz signal, which is transmitted to the nanomaterial via coplanar probes. The measured material is a 30 μm × 30 μm piece, with lattice constants of $a_x = 800$ nm and $a_y = 300$ nm in the lateral and vertical directions, respectively, and both the base and the height of the triangular antidots are 150 nm. The experiment is performed at room temperature. Similar results are obtained in other materials with different structural parameters.

Although we have not tested the material at frequencies higher than 50 GHz, from the working principle we expect the cut-off frequency to be much higher, possibly up to hundreds of GHz or even in the THz regime. The large area, in combination with the in-plane layout of the material, enables straightforward and efficient coupling to high-frequency microwaves. Moreover, microwaves travelling along the normal direction of the nanomaterial surface yield the most efficient coupling, while coupling has to be achieved in specific ways (including using antennae) in a conventional vertical device. From the material point of view, to the best of our knowledge, this is the first artificial electronic nanomaterial that operates at room temperature.

An external noise signal can also induce a guided net flow of electrons in the upward direction and generate a direct voltage [25]. In many aspects, the ratchet effect in the artificial nanomaterial resembles the photovoltaic effect in some natural crystals [15–17]. In our man-made artificial crystals, however, we are able to design (adjust) the size and shape of the symmetry-breaking elemental units, as well as the lattice constants. Such flexibility may also provide a new route in further studies of the photovoltaic effect, and possibly some biological phenomena as well.

6 Conclusions

We have demonstrated a new type of nonlinear nano-rectifier, which generates a strong ratchet effect. Based on a similar microscopic mechanism, we have also constructed, to the best of our knowledge, the first artificial electronic nanomaterial that operates at room temperature. The facts that they can be reproducibly fabricated and can function at room temperature as well as at 50 GHz suggest that the ballistic rectifier and the artificial nanomaterial might be very close to practical applications.

ACKNOWLEDGEMENTS The work performed at Munich was supported through the Deutsche Forschungsgemeinschaft (SFB 348). Collaboration with A. Lorke, J.P. Kotthaus, A. Kriele, S. Manus, M. Streibl, W. Wegscheider and M. Bichler is gratefully acknowledged. The author also thanks the Alexander von Humboldt Foundation for a Research Fellowship. A. Löfgren, I. Maximov, P. Omling, L. Samuelson, W. Seifert, I. Shorubalko and H.Q. Xu at Lund University and H. Zirath at the Department of Microwave Technology, Chalmers University of Technology, Göteborg, Sweden, also contributed greatly to the work. The experiments at Lund were supported by the Swedish Natural Science Research Council, the Swedish Research Council for Engineering Science, the "Quantum Materials" program of the Swedish Foundation for Strategic Research and the European Commission through the LTR research project Q-SWITCH.

REFERENCES

1 M.O. Magnasco: Phys. Rev. Lett. **71**, 1477 (1993)
2 J. Prost, J.-F. Chauwin, L. Peliti, A. Ajdari: Phys. Rev. Lett. **72**, 2652 (1994)
3 C.R. Doering, W. Horsthemke, J. Riordan: Phys. Rev. Lett. **72**, 2984 (1994)
4 P. Hänggi, R. Bartussek: In *Nonlinear Physics of Complex Systems*, ed. by J. Parisi, S.C. Müller, W. Zimmermann, Lecture Notes in Physics, Vol. 476 (Springer, Berlin, Heidelberg 1996)
5 F. Jülicher, A. Ajdari, J. Prost: Rev. Mod. Phys. **69**, 1269 (1997)
6 P. Reimann, M. Grifoni, P. Hänggi: Phys. Rev. Lett. **79**, 10 (1997)
7 R.D. Astumian: Science **276**, 917 (1997)
8 R.D. Astumian, F. Moss (Eds.): Chaos **8**, 533 (1998)
9 P. Reimann: Phys. Rep. **361**, 57 (2002)
10 K. Kitamura, M. Tokunaga, A.H. Iwane, T. Yanagida: Nature **397**, 129 (1999)
11 D. Erta: Phys. Rev. Lett. **80**, 1548 (1998)
12 T.A.J. Duke, R.H. Austin: Phys. Rev. Lett. **80**, 1552 (1998)
13 C.F. Chou, O. Bakajin, S.W.P. Turner, T.A.J. Duke, S.S. Chan, E.C. Cox, H.G. Craighead, R.H. Austin: Proc. Nat. Acad. Sci. USA **96**, 13 762 (1999)
14 A. van Oudenaarden, S.G. Boxer: Science **285**, 1046 (1999)
15 A.M. Glas, D. von der Linde, T.J. Negran: Appl. Phys. Lett. **25**, 233 (1974)
16 V.I. Belinicher, B.I. Sturman: Sov. Phys. Usp. **23**, 199 (1980)
17 B.I. Sturman, V.M. Fridkin: *The Photovoltaic and Photorefractive Effects in Noncentrosymmetric Materials* (Gordon and Breach, Philadelphia 1992)
18 A. Lorke, S. Wimmer, B. Jager, J.P. Kotthaus, W. Wegscheider, M. Bichler: Physica B **249**, 312 (1998)
19 A.M. Song, A. Lorke, A. Kriele, J.P. Kotthaus, W. Wegscheider, M. Bichler: Phys. Rev. Lett. **80**, 3831 (1998)
20 H. Linke, W. Sheng, A. Löfgren, H.Q. Xu, P. Omling, P.E. Lindelof: Europhys. Lett. **44**, 341 (1998)
21 H. Linke, T.E. Humphrey, A. Lofgren, A.O. Sushkov, R. Newbury, R.P. Taylor, P. Omling: Science **286**, 2314 (1999)
22 J. Imry: In *Directions in Condensed Matter Physics*, ed. by G. Grinstein, G. Mazenko (World Scientific, Singapore 1986) pp. 101; C.W.J. Beenakker, H. Van Houten: Solid State Phys. **44**, 1 (1991); S. Datta: *Electronic Transport in Mesoscopic Systems* (Cambridge University Press, Cambridge 1995)
23 A.M. Song: Phys. Rev. B **59**, 9806 (1999)
24 A.M. Song, A. Lorke, A. Kriele, J.P. Kotthaus, W. Wegscheider, M. Bichler: In Proc. 24th Int. Conf. Phys. Semicond., ed. by D. Gershoni (World Scientific, Singapore 1998)

25 A. Löfgren, I. Shorobalko, P. Omling, A.M. Song: to be published
26 R. Landauer: IBM J. Res. Dev. **1**, 223 (1957); ibid.: Philos. Mag. **21**, 863 (1970)
27 M. Büttiker: Phys. Rev. Lett. **57**, 1761 (1986); ibid.: IBM J. Res. Dev. **32**, 317 (1988)
28 M.L. Roukes, A. Scherer, S.J. Allen Jr., H.G. Craighead, R.M. Ruthen, E.D. Beebe, J.P. Harbison: Phys. Rev. Lett. **59**, 3011 (1987)
29 G. Timp, H.U. Baranger, P. deVegvar, J.E. Cunningham, R.E. Howard, R. Behringer, P.M. Mankiewich: Phys. Rev. Lett. **60**, 2081 (1988)
30 H. van Houten, C.W.J. Beenakker, P.H.M. van Loosdrecht, T.J. Thornton, H. Ahmed, M. Pepper, C.T. Foxon, J.J. Harris: Phys. Rev. B **37**, 8534 (1988)
31 C.J.B. Ford, S. Washburn, M. Büttiker, C.M. Knoedler, J.M. Hong: Phys. Rev. Lett. **62**, 2724 (1989)
32 C.W.J. Beenakker, H. van Houten: Phys. Rev. B **39**, 10 445 (1989)
33 L.W. Molenkamp, A.A.M. Staring, C.W.J. Beenakker, R. Eppenga, C.E. Timmering, J.G. Williamson, C.J.P.M. Harmans, C.T. Foxon: Phys. Rev. B **41**, 1274 (1990)
34 J. Spector, H.L. Stormer, K.W. Baldwin, L.N. Pfeiffer, K.W. West: Appl. Phys. Lett. **56**, 1290 (1990)
35 A. Palevski, C.P. Umbach, M. Heiblum: Appl. Phys. Lett. **55**, 1421 (1989)
36 R. Taboryski, A.K. Geim, M. Persson, P.E. Lindelof: Phys. Rev. B **49**, 7813 (1994)
37 R.I. Hornsey, A.M. Marsh, J.R.A. Cleaver, H. Ahmed: Phys. Rev. B **51**, 7010 (1995)
38 D.R.S. Cumming, J.H. Davies: Appl. Phys. Lett. **69**, 3363 (1996)
39 A. Messica, A. Soibel, U. Meirav, A. Stern, H. Shtrikman, V. Umansky, D. Mahalu: Phys. Rev. Lett. **78**, 705 (1997)
40 K. Hieke, M. Ulfward: Phys. Rev. B **62**, 16 727 (2000)
41 P.F. Bagwell, T.P. Orlando: Phys. Rev. B **40**, 1456 (1989)
42 L.I. Glazman, A.V. Khaetskii: Europhys. Lett. **9**, 263 (1989)
43 O. Heinonen, M.D. Johnson: Phys. Rev. Lett. **71**, 1447 (1993); M.D. Johnson, O. Heinonen: Phys. Rev. B **51**, 14 421 (1995)
44 M. Büttiker: J. Phys. Condens. Matter **5**, 9361 (1993)
45 S. Komiyama, H. Hirai: Phys. Rev. B **54**, 2067 (1996)
46 S. Ulreich, W. Zwerger: Superlattices Microstruct. **23**, 719 (1998)
47 H.Q. Xu: Appl. Phys. Lett. **78**, 2064 (2001)
48 C.W.J. Beenakker, H. van Houten: Phys. Rev. Lett. **63**, 1857 (1989)
49 A.M. Song, S. Manus, M. Streibl, A. Lorke, J.P. Kotthaus, W. Wegscheider, M. Bichler: Superlattices Microstruct. **25**, 269 (1999)
50 A.M. Song, A. Lorke, J.P. Kotthaus, W. Wegscheider, M. Bichler: Superlattices Microstruct. **25**, 149 (1999)
51 A.M. Song, P. Omling, L. Samuelson, W. Seifert, I. Shorubalko, H. Zirath: Jpn. J. Appl. Phys. **40**, L909 (2001)
52 P. Ramvall, N. Carlsson, P. Omling, L. Samuelson, W. Seifert, M. Stolze, Q. Wang: Appl. Phys. Lett. **68**, 1111 (1996)
53 Y. Hirayama, S. Tarucha: Appl. Phys. Lett. **63**, 2366 (1996)
54 I. Shorubalko, A. Löfgren, P. Omling, A.M. Song: to be published
55 A.M. Song, P. Omling, L. Samuelson, W. Seifert, I. Shorubalko, H. Zirath: Appl. Phys. Lett. **79**, 1357 (2001)